ASTRONOMY
AND
ASTROPHYSICS

An X-ray study of the dipping low mass X-ray binary XB 1323−619

M. Bałucińska-Church[1], M.J. Church[1], T. Oosterbroek[2], A. Segreto[3], R. Morley[1], and A.N. Parmar[2]

[1] School of Physics and Astronomy, University of Birmingham, Birmingham, B15 2TT, UK
[2] Astrophysics Division, Space Science Department of ESA, ESTEC, Postbus 299, 2200 AG Noordwijk, The Netherlands
[3] Instituto IFCAI, via La Malfa 153, I-90146 Palermo, Italy

Abstract. During a BeppoSAX observation of the low-mass X-ray binary dip source XB 1323−619 a total of 10 type I X-ray bursts and parts of 12 intensity dips were observed. During non-bursting, non-dipping intervals, the 1.0–150 keV BeppoSAX spectrum can be modelled by a cutoff power-law with a photon index of 1.48 ± 0.01, a cutoff energy of $44.1^{+5.1}_{-4.4}$ keV together with a blackbody with kT of 1.77 ± 0.25 keV contributing $\sim$15% of the 2–10 keV flux. Absorption equivalent to $3.88 \pm 0.16 \times 10^{22}$ atom cm^{-2} is required. The dips repeat with a period of 2.938 ± 0.020 hr and span 40% of the orbital cycle. During dips the maximum reduction in 2–10 keV intensity is $\sim$65%. The spectral changes during dips are complex and cannot be modelled by a simple absorber because of the clear presence of part of the non-dip spectrum which is not absorbed. Spectral evolution in dipping can be well modelled by progressive covering of the cutoff power-law component which must be extended, plus rapid absorption of the point-source blackbody. One of the bursts is double and 4 of the bursts occurred during dipping intervals. These bursts have 2–10 keV peak count rates reduced by only 22% on average from those occurring outside the dips, and are not heavily absorbed. One explanation for this lack of absorption is that the bursts temporarily ionize the absorbing material responsible for the dips.

Key words: X-rays: stars – stars: individual: XB 1323-619 – stars: neutron – stars: binaries: close – accretion, accretion disks

1. Introduction

A significant fraction of low-mass X-ray binaries (LMXB) exhibit periodic dips in their X-ray intensity. The dips recur at the orbital period of the system and are believed to be caused by periodic obscuration of a central X-ray source by structure located in the outer regions of an accretion disk (White & Swank 1982). The depth, duration and spectral properties of the dips vary from source to source and from cycle to cycle (e.g. Parmar & White 1988). Determination of the spectral evolution in dipping allows not only the structure and dynamics of the outer regions of the accretion disk and the properties of the absorbing material,

but also the geometry and nature of the emission regions, to be investigated (see Church et al. 1997, 1998a,b). In the LMXB dip sources, the spectral changes during dips are complex and can not be described by simple absorption of one-component emission but can be described by assuming two emission components: one point-like blackbody from the surface of the neutron star, and the other extended Comptonized emission from an Accretion Disk Corona (ADC) (Church & Bałucińska-Church 1993, 1995). In some sources, dipping is well explained in terms of a relatively small absorber which covers the point-like emission but does not absorb the extended emission to a large extent. In another group of dip sources, the dip spectra indicate the presence of excesses at $\lesssim$4 keV, i.e. clear evidence that part of the spectrum is not absorbed (Parmar et al. 1986; Courvoisier et al. 1986; Smale et al. 1992; Church et al. 1997). XB 1323−619 belongs to this group (Parmar et al. 1989). The dip spectra of these sources have often been fitted by a technique in which the non-dip spectral form is split into two parts each having the form of non-dip emission, but only one of which suffers extra absorption, while the other has a normalization which decreases markedly in dipping, often by a factor of 10. This may be called 'absorbed + unabsorbed' modelling. Explanations for the apparent change in normalization have been based on electron scattering, partial covering by the absorber and fast variations of column density (Parmar et al. 1986); however, it has been difficult to explain the large changes convincingly. For example, a large degree of electron scattering is unlikely in the outer accretion disk where the ionization state is low as demonstrated by the observed occurrence of photoelectric absorption in dipping. An alternative approach based on the two-component model (above) for the dip sources has been suggested (Church et al. 1997). In this group of sources, the absorber is extended and often of larger angular extent than all emission regions. Thus in dipping, the point-like blackbody region is covered immediately whereas the extended Comptonized emission region is progressively covered by the absorber. This approach can explain the complex behaviour in several sources (Church et al. 1997, 1998a,b), and provides a simple explanation in which the unabsorbed part of the dip spectrum originates from the uncovered emission as the extended absorber moves across the extended emission region.

XB 1323−619 is a faint (∼3 mCrab), poorly studied LMXB that exhibits 2.93 hour periodic intensity dips and X-ray bursts. The source was first detected by *Uhuru* and *Ariel V* (Forman et al. 1978; Warwick et al. 1981) and the dips, bursts and a soft excess during dips were discovered using EXOSAT (van der Klis et al. 1985; Parmar et al. 1989, hereafter P89). Recently, ∼1 Hz quasi-periodic oscillations have been discovered in the persistent emission, the dips and the bursts from XB 1323−619 (Jonker et al. 1999). The EXOSAT Medium Energy 1–10 keV non-dip spectrum could be modelled by either a power-law with a photon index of 1.53 ± 0.07 and absorption, N_{H} equivalent to $(4.0 \pm 0.3) \times 10^{22}$ atom cm^{-2}, or a thermal bremsstrahlung with a temperature of 26^{+14}_{-6} keV (P89). During the dips, which typically last for 40% of the orbital cycle, the X-ray intensity varies irregularly with a minimum of ∼50% of the average value outside of the dips. During the EXOSAT observation the bursts repeated every 5.30–5.43 hr. XB 1323−619 lies close to the galactic plane ($l_{II} = 307.0°$, $b_{II} = 0.4°$ and the average column density in this direction is $\sim 1.4 \times 10^{22}$ atom cm^{-2} (using Stark et al. 1995). The region of sky containing XB 1323−619 is complex with ten point sources detected in previous EXOSAT Channel Multiplier Array (CMA) and *Einstein* imaging observations (see Fig. 4 of P89). On the basis of an extreme hardness ratio, P89 proposed that source D, detected during *Einstein* Imaging Proportional Counter (IPC) and High Resolution Imager observations (HRI), is probably XB 1323−619. The count rates in these observations are too low to detect dipping clearly. The identification of source D with XB 1323−619 was recently confirmed when Smale (1995) discovered a faint ($K' = 17$) variable IR object within the uncertainty region for source D during a short (1.5 hr) observation using the Infrared Imaging Spectrometer at the Anglo-Australian Telescope.

We present a detailed study of the XB 1323−619 X-ray spectrum and its evolution during dips using results obtained with BeppoSAX. We compare the properties of bursts that occurred during dipping with those outside dipping intervals. Spectral fitting results from the previously unpublished 1994 ASCA observation of XB 1323−619 are presented and compared with the BeppoSAX results. The serendipitous detection of a pulsing source within the XB 1323−619 field using BeppoSAX is reported in Angelini et al. (1998).

2. Observations

2.1. BeppoSAX

Data from the Low-Energy Concentrator Spectrometer (LECS; 0.1–10 keV; Parmar et al. 1997), Medium-Energy Concentrator Spectrometer (MECS; 1.3–10 keV; Boella et al. 1997), High Pressure Gas Scintillation Proportional Counter (HPGSPC; 5–120 keV; Manzo et al. 1997) and the Phoswich Detection System (PDS; 15–300 keV; Frontera et al. 1997) on-board BeppoSAX are presented. All these instruments are coaligned and collectively referred to as the Narrow Field Instruments, or NFI. The MECS consists of three identical grazing incidence telescopes with imaging gas scintillation proportional counters in their focal planes, however prior to the observation of XB 1323−619

one of the detectors had failed. The LECS uses an identical concentrator system as the MECS, but utilizes an ultra-thin entrance window and a driftless configuration to extend the low-energy response to 0.1 keV. The non-imaging HPGSPC consists of a single unit with a collimator that is alternatively rocked on- and off-source to monitor the background spectrum. The non-imaging PDS consists of four independent units arranged in pairs each having a separate collimator. Each collimator can be alternatively rocked on- and off-source to monitor the background.

The region of sky containing XB 1323−619 was observed by BeppoSAX between 1997 August 22 17:06 and August 24 02:02 UTC. Good data were selected from intervals when the elevation angle above the Earth's limb was $>4°$ and when the instrument configurations were nominal, using the SAXDAS 1.3.0 data analysis package. The standard collimator dwell time of 96 s for each on- and off-source position was used, together with rocking angles of $180'$ and $210'$ for the HPGSPC and PDS, respectively. The exposures in the LECS, MECS, HPGSPC, and PDS instruments are 15 ks, 70 ks, 28 ks, and 28 ks, respectively. LECS and MECS data were extracted centered on the position of XB 1323−619 using radii of $8'$ and $4'$, respectively. Background subtraction in the imaging instruments was performed using standard files, but is not critical for such a bright source. Background subtraction in the non-imaging instruments was carried out using data from the offset intervals.

2.2. ASCA

The ASCA instrumentation consists of two Solid State Imaging Spectrometers SIS0 and SIS1 (0.6–10 keV), and two Gas Imaging Spectrometers GIS2 and GIS3 (0.8–10 keV, Tanaka et al. 1994). The energy resolution of the GIS is similar to that of the BeppoSAX LECS and MECS in the overlapping energy range, while that of the SIS is a factor of a few better, except at the lowest energies.

ASCA observed the XB 1323−619 region on 1994 August 04 between 12:28 and 20:10 UTC with a GIS exposure of 22 ks. GIS data were screened to remove regions of high particle background, to restrict elevation above the rim of the Earth to $>5°$, particle rigidity to more than 6 GeV c^{-1}, the radiation belt parameter to less than 200 count s^{-1}, and angular deviation to less than $0.014°$. The calibration source and outer ring were removed from the image, and rise-time rejection applied. Source and background data were selected from diametrically opposite $6'$ radius regions. Two bursts and parts of two dips were observed.

3. Results

3.1. The X-ray lightcurve

Fig. 1 shows the background-subtracted 2–10 keV MECS lightcurves of XB 1323−619 with a binning of 64 s. The scaling is chosen to show the dipping clearly in the upper panel and the bursting clearly in the lower panel. Parts of 12 dips were seen as irregular reductions in intensity as well as 10 X-ray bursts.
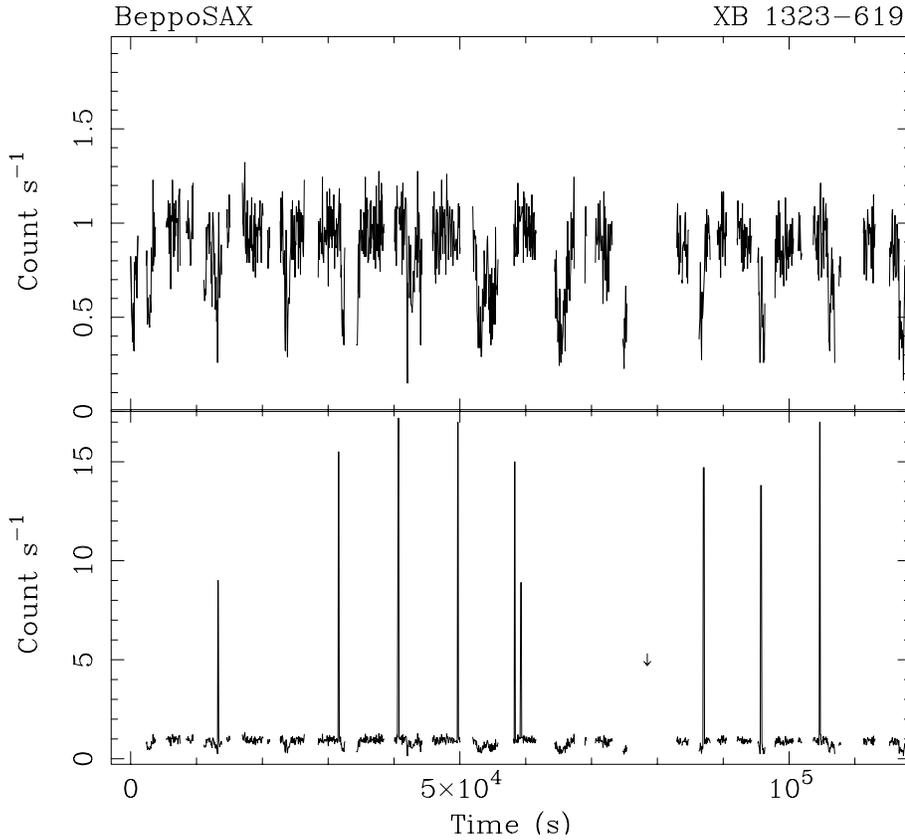
Fig. 1. MECS 2–10 keV lightcurves of XB 1323−619 with a binning time of 64 s. In the upper panel the bursts are removed in order to show the dips clearly. The position of the burst observed by the LECS but not by the MECS is indicated by an arrow

One of these is a double burst, and one burst was observed by the LECS, but not by the MECS which was switched-off for one satellite orbit during the observation for technical reasons. With the binning used, the apparent heights of the bursts (lasting ~100 s) are substantially reduced from their true heights obtained from a light curve with much shorter binning (less than 4 s). Since we wish to show clearly the differences between the bursts that occur in non-dip emission and those coinciding with dips (Sect. 4), we have corrected the burst heights in Fig. 1 to their values with binning less than 4 s. Bursts and dips are not strongly evident in the HPGSPC and PDS lightcurves due to the poorer signal to noise ratio of these instruments and the energy dependence of these features.

It can be seen from Fig. 1 that dipping is not 100% deep in the band 2–10 keV, and so the source differs from XB 1916-053, for example (Church et al. 1998b), in which dipping is usually 100%. To investigate this, light curves were also extracted in various energy bands within the range of the MECS. The results showed dipping to be 100% deep (at its deepest point) in the band below 2.3 keV, decreasing systematically with increasing energy, i.e. 67% in the band 3–6 keV and 57% in the band 6–10 keV. However, the count rate was low, particularly in the lowest band and the Poisson errors large. If dipping is 100% deep at the lowest energies, the consequence is that the overall size of the absorber must be larger than the largest emission region. This is further discussed in Sect. 5.

Fig. 2 shows the 2.0–10 keV background subtracted MECS lightcurve and hardness ratio folded on the best-fit dip period
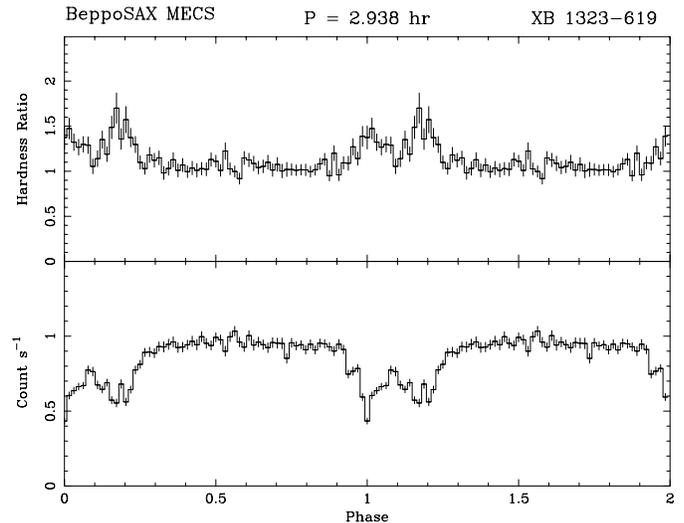

Fig. 2. The XB 1323−619 lightcurve and hardness ratio folded on the dip period and displayed over repeated cycles for clarity. Intervals corresponding to X-ray bursts are excluded. Dipping activity is clearly seen as increases in hardness ratio

given below. Intervals corresponding to X-ray bursts have been excluded. The hardness ratio is defined as the count rate in the energy range 4.5–10.0 keV divided by that in the range 1.8–4.5 keV. Dipping activity is clearly seen as increases in hardness ratio consistent with the energy-dependence of dipping and is

evident between phases 0.9 to 1.3 (where phase 0.0 is defined as the epoch of deepest dipping).

The dip period was determined Using MECS data from which the bursts were excluded, and found to be 2.938 ± 0.020 hr. The period and 1σ uncertainty were derived by estimating the times corresponding to the center of each dip from template fits and fitting the resulting arrival times to a linear relation with cycle number. The folded templates were updated as more refined values of the period were obtained until the fitting converged. The minimum in the folded light curve occurs at MJD 50682.719 ± 0.0045. The period is consistent with that derived from the 1985 February EXOSAT observation of 2.932 ± 0.005 hr (P89). ASCA observed only two dips, one of which was broken by data gaps, and the dip period cannot be reliably obtained.

3.2. X-ray spectra

The spectrum of non-dip emission was investigated by simultaneously fitting data from all the BeppoSAX NFI. Time intervals corresponding to bursts were first removed, and then data selected with phases between 0.3 and 0.9 using the ephemeris given in Sect. 3.1. This gives background-subtracted count rates of 0.41, 1.12, 2.59 and 2.16 count s^{-1} for the LECS, MECS, HPGSPC and PDS, respectively. Spectral evolution in dipping was investigated using MECS data only since the dips are not strongly seen at higher energies and there are too few counts in the LECS to contribute meaningfully. After initial trials, MECS dip spectra were extracted with count rates between 0.3–0.6 count s^{-1}, 0.6–0.75 count s^{-1} and 0.75–0.85 count s^{-1} after first binning the data in 128s intervals. Given the count rate of the source, a larger number of dip spectra would not be sensible. The LECS and MECS spectra were rebinned to oversample the full width at half maximum of the energy resolution by a factor of 3, and additionally LECS data were rebinned to a minimum of 20 counts per bin and MECS data to 60 counts per bin to allow use of the χ^2 statistic. LECS data were only used between 1–5 keV and MECS data between 1.8–10.0 keV where the instrument responses are well determined. The HPGSPC and PDS data were rebinned using standard binnings in the bands 7–20 keV and 13–150 keV, respectively. In the following, the photoelectric absorption cross sections of Morrison & McCammon (1983) were used incorporating the Solar abundances of Anders & Grevesse (1989).

In order to understand the spectrum of a dip source the spectral model must give acceptable fits to both the non-dip and dip spectra. Since dips are almost certainly due to obscuration by intervening material, a satisfactory model should fit the dip spectra without requiring any of the parameters that characterize the source emission such as the temperature or power-law index to be changed. Normally, the procedure followed consists of obtaining these parameters from fitting the non-dip spectrum. However, in the case of weak sources, the non-dip spectrum alone may not constrain parameters sufficiently. This is the case here, and instead, the NFI non-dip spectra and the 3 dip spectra were fitted simultaneously. This approach proved successful in discriminating between various models, and providing a good fit to all spectra with our best model.

Initially, simple models were tried, including absorbed power-law, thermal bremsstrahlung and cutoff power-law: $E^{-\alpha}\exp-(E/E_{\rm co})$ models. Factors were included in the spectral fitting to allow for normalization uncertainties between the instruments; values of these factors were similar to those found for other sources. The power-law model gave an unacceptable fit with a χ^2 of 1110/397, and strong discrepancies between model and data above 40 keV where there is down-curving of the spectrum. The bremsstrahlung model similarly did not provide an acceptable fit with a χ^2 of 995/396. Although the fit to the non-dip data alone was only marginally unacceptable, there were large discrepancies between data and model for deeper dip data. The cutoff power-law was also unacceptable with a χ^2 of 665/396. In all cases, there is an unabsorbed component in the spectra at low energies (or soft excess), most obvious in the deeper dip spectra. Thus, there was little change in the low energy cutoff of the spectrum in dipping compared with the non-dip spectrum.

Next, the model frequently applied to the dip sources with an unabsorbed component at low energies was tried (e.g. Parmar et al. 1986). The non-dip model consisting of a cutoff power-law was split for the dip spectra into two cutoff power-laws having identical spectral parameters except for the column densities and normalizations. In the one component, the column density was allowed to vary, in the other, the column density was frozen at the non-dip value; both normalizations were free. For the non-dip spectrum, this model reduces to a single component. This model fitted the spectra well with an overall χ^2 for the fit of 392/390. The absorbed component has an increasing $N_{\rm H}$ in dipping with approximately constant normalization; however for the unabsorbed component there is a large change in normalization which decreases by a factor of ~2 in the deepest dip spectrum of Fig. 4 (intensity band 0.3–0.6 count s^{-1}). We also sub-divided this band making a spectrum for 0.3–0.4 count s^{-1} for which the normalization change was 2.5. We are not able to explain such a decrease in normalization: for example, in Fig. 5, there is no evidence that extensive electron scattering of X-rays takes place in the absorber which would be seen as an energy-independent shift between the deep dip and non-dip spectra shown.

However, for the first time, BeppoSAX offers the ability to test this model more rigorously since the normalization decrease, if real, implies that the PDS intensity (at energies where absorption plays no part) would have to decrease substantially between non-dip and deep dipping, which it clearly does not. Fitting the deep dip model obtained above to the PDS deep dip spectrum has a χ^2 of 27.4/7 for the data between 20 and 50 keV. Thus, this model is not able to fit the PDS data. The present work on XB 1323−619 and previous work on other sources with an unabsorbed part of the spectrum (Church et al. 1997, 1998a,b) where the normalization decrease is typically a factor of 10, provide evidence that the change in normalization is unreal, and is due to the application of an inappropriate model. Thus

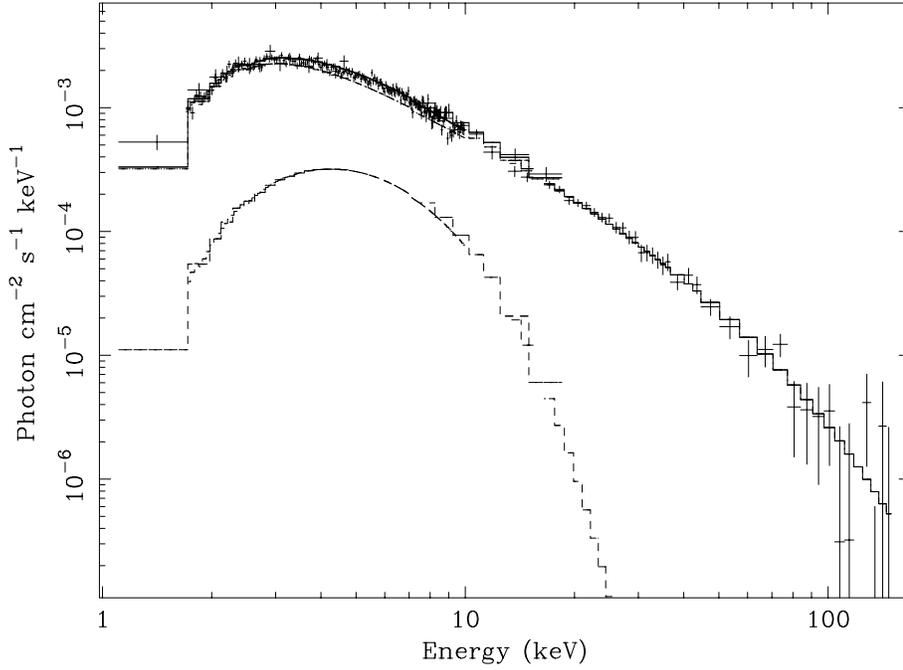BeppoSAX NFI   XB 1323−619

Fig. 3. The non-dip NFI XB 1323−619 spectrum fitted with the absorbed cutoff power-law and blackbody model discussed in the text. The data have been rebinned to aid clarity. The total model and the contribution of the blackbody component are shown separately

Table 1. Spectral fitting results obtained by simultaneously fitting the BeppoSAX NFI non-dip spectrum and 3 dip spectra using various models (see text). N_H is in units of 10^{22} atom cm^{-2}. 90% confidence limits are given

Model	N_H	kT (keV)	α	E_{co} (keV)	χ^2/dof
Power-law	4.71 ± 0.18	...	1.81 ± 0.01	...	1110/397
Bremsstrahlung	3.52 ± 0.17	23.4 ± 1.88	...	...	995/396
Cutoff power-law (simple absorber)	3.98 ± 0.18	...	1.43 ± 0.01	$40.9^{+4.2}_{-3.7}$	665/396
Cutoff power-law + cutoff power-law	4.05 ± 0.16	...	1.43 ± 0.01	$40.5^{+4.1}_{-3.6}$	392/390
Cutoff power-law (prog. covering)	4.26 ± 0.16	...	1.49 ± 0.01	$44.0^{+4.9}_{-4.2}$	453/393
Cutoff power-law + blackbody (prog. covering)	3.88 ± 0.16	1.77 ± 0.25	1.48 ± 0.01	$44.1^{+5.1}_{-4.4}$	401/387

this fitting is shown in Table 1 only for completeness, as a cutoff power-law + cutoff power-law model.

We next tried the progressive covering model, which consists of a point-like blackbody and an extended Comptonization term, with progressive covering of the extended component in dipping (e.g. Church et al. 1998b). The model flux may be written:

$$e^{-\sigma_{MM}N_H} \left(I_{BB}e^{-\sigma_{MM}N_H^{BB}} + I_{CPL} \left(f \, e^{-\sigma_{MM}N_H^{CPL}} + (1-f) \right) \right)$$

Here I_{BB} and I_{CPL} are the normalizations of the blackbody and cutoff power-law components, N_H^{BB} and N_H^{CPL} are the column densities for each component during dipping (additional to the non-dip N_H), and f is the covering fraction. This model gave an acceptable χ^2 of 401/387. The cutoff power-law parameters are provided essentially by the deep dip spectrum in which the blackbody is totally absorbed, whereas the blackbody parameters are provided by the non-dip spectrum.

Removing the blackbody term and re-fitting simultaneously gave a significantly worse χ^2 of 453/393. An F-test shows that the additional component is significant with >>99.9% confidence. Moreover when χ^2 is obtained for the spectra fitted indi-

vidually, using the best simultaneous solution, the fits get worse for deeper dipping with a χ^2 of 100/47 in the deepest dip spectrum. Closer examination of the non-dip and first dip spectra (shallow dipping) reveals that absorption is clearly taking place in the band 5–10 keV (see Fig. 4), indicating that a component of the spectrum in this energy band is rapidly removed in dipping. The spectral model with progressive covering of a cutoff power-law only *does not allow* absorption in this band, since in shallow dipping, the covering fraction is less than 40%, and N_H for the cutoff power-law is low (see Table 2). To produce the observed decrease in count rate at 5 keV of 20% for the shallow dip spectrum by progressive covering of the cutoff power-law alone, a column density of more than 20×10^{22} atom cm^{-2} would be required, several times larger than N_H for this component. However, when the blackbody is added, this component being point-like is immediately covered and has high N_H and so can be absorbed in the band 5–10 keV in shallow dipping.

The best-fit non-dip parameters (for the blackbody + cutoff power-law model) are summarised in Table 1 and the fit to the 4 instruments shown in Fig. 3. The good fit of this model
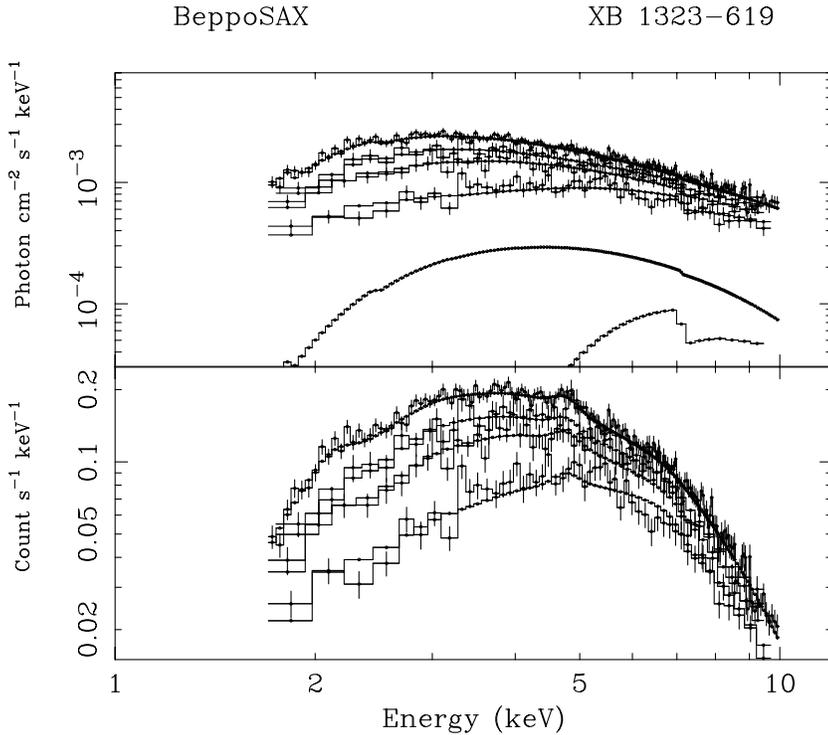
BeppoSAX   XB 1323−619

Fig. 4. Progressive covering fits to the MECS non-dip and 3 dip spectra given in Table 2. The lower panel shows the spectra and total model folded through the instrument response. The upper panel shows the observed counts spectra with total model and the blackbody components (lower curves), omitting the cutoff power-law for clarity. Only the blackbody contributions to the non-dip and shallow dip spectrum are shown, as the contributions in the other cases are too small to be included

Table 2. Best fits to the dip spectra. N_H is in units of 10^{22} atom cm^{-2} for both the spectral components. 90% confidence limits are given

Spectrum	MECS ct rate (s^{-1})	N_H^{BB}	N_H^{CPL}	f	χ^2/dof
Non-dip	...	3.88±0.16	3.88±0.16	0.0	150/163
Shallow dip	0.75–0.85	63^{+110}_{-28}	7.0±1.1	0.376±0.085	41/48
Medium dip	0.60–0.75	2.2×10^4	13.8±1.8	0.423±0.036	46/48
Deep dip	0.30–0.60	6.1×10^4	26.7±2.1	0.665±0.019	75/51

shown in Fig. 3 confirms the existence of a high-energy spectral break strongly supporting the Comptonized nature of the non-thermal emission and allows parameters of the Comptonizing region to be derived. In the 2–10 keV energy range, the blackbody contributes 14% of the total luminosity. The best-fit N_H of $(3.88 \pm 0.16) \times 10^{22}$ atom cm^{-2} is somewhat higher than Stark et al. (1995) value of $\sim 1.4 \times 10^{22}$ atom cm^{-2}, suggesting the presence of absorber intrinsic to the source. Including a narrow Fe line in the non-dip fitting did not bring any improvement in fit quality, and the 90% confidence upper limit to the equivalent width (EW) of a narrow line at 6.4 keV is 48 eV. However, for the shallow and medium dip spectra, the fits *were marginally improved*, with EW < 100 eV and EW < 160 eV in these two cases.

In Fig. 4, the fits of the progressive covering model (from simultaneous fitting) to the non-dip and each of the MECS dip spectra are shown, and the results are summarised in Table 2. During the fitting the values of α, kT, E_{co} and the normalizations of the two components were chained. χ^2 values were obtained by applying the best-fit solution to each spectrum individually. The fit to the deepest dip spectrum is not quite so good as to the other spectra because of the reduced quality of the spectrum. It

can be seen that the blackbody column increases rapidly, consistent with absorption of a point-like source in the denser regions of the absorber. In contrast, the non-thermal component is more slowly and progressively covered during dipping intervals, with *f* rising smoothly from zero to $\sim$0.67. The systematic increase of *f* as dipping deepens is consistent with a large absorbing region moving progressively across an extended emission component, and the unabsorbed part of the spectrum is simply the uncovered part of the emission. The smaller increase of column density for the extended component compared with the point-like blackbody is as expected, since the blackbody will be absorbed by denser regions in the absorber while the non-thermal component measures an average column density integrated across the absorber.

3.3. ASCA spectrum

The ASCA non-dip spectrum selected from the GIS2 intensity band between 0.7–0.85 count s^{-1} was also fitted using a blackbody and power-law model (the ASCA data does not extend to high enough energies to observe the cutoff). In this case, kT_{bb} is $1.85^{+0.31}_{-0.18}$ keV and the photon index is $2.46^{+2.06}_{-1.48}$. If a cutoff
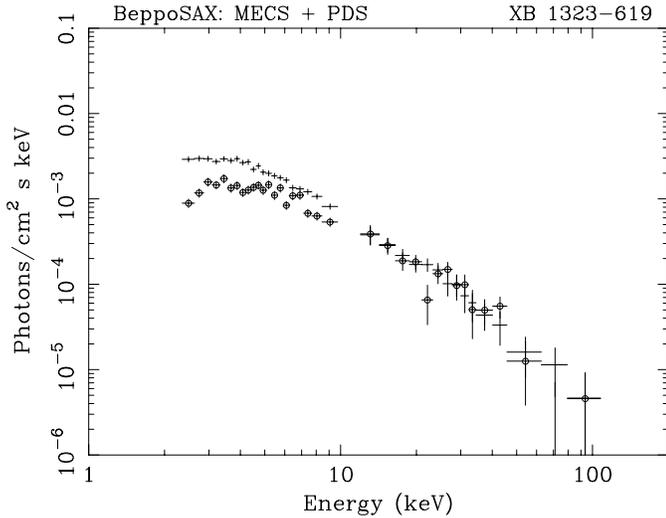
Fig. 5. Non-dip and deep dip (circles) MECS and PDS spectra illustrating the lack of evidence for dipping $\gtrsim 20$ keV. The spectra have been deconvolved using the best-fit progressive covering model with parameters given in Tables 1 and 2

Table 3. Burst properties. Bursts 5 and 6 comprise the double burst and burst 7 was not observed by the MECS. Phase is defined using the ephemeris given in Sect. 3.1. Dips occur between phases 0.9–1.3

Burst No.	Time (1997) Day hr:mn	MECS counts	Exp. (s)	Dip phase	Comment
1	Aug 22 20:49	297	69.6	0.22	Dip
2	Aug 23 01:54	439	98.3	0.94	Dip
3	Aug 23 04:25	525	96.2	0.80	Non-dip
4	Aug 23 06:56	539	99.3	0.66	Non-dip
5	Aug 23 09:20	504	96.9	0.48	Non-dip
6	Aug 23 09:36	137	34.8	0.56	Non-dip
7	Aug 23 14:55	. . .	. . .	0.38	Non-dip
8	Aug 23 17:19	372	84.0	0.19	Dip
9	Aug 23 19:44	292	66.5	0.01	Dip
10	Aug 23 22:13	437	82.1	0.85	Non-dip

power-law is used with α and E_{co} fixed at the BeppoSAX best-fit values, then kT_{bb} is $1.72 \pm^{0.38}_{0.12}$ keV in excellent agreement with the BeppoSAX results. Thus the overall spectral shape during the ASCA observation is very similar to that observed by BeppoSAX.

3.4. High energy variations

Fig. 4 shows that significant dipping takes place at 10 keV. A PDS spectrum was extracted corresponding to the same time intervals used to select the deepest dip MECS spectrum. The mean 15–50 keV non dip PDS count rate is 1.48 ± 0.03 s^{-1}, compared with 1.35 ± 0.14 s^{-1} in deep dipping. Fig. 5 shows the MECS and PDS non-dip and deep dip spectra, from which it is clear that absorption continues up to ~ 20 keV; however at higher energies there is no evidence for any substantial energy-independent decrease of flux in the PDS, i.e. for any large degree of electron scattering in the absorber. A limit of $10 \pm 10\%$ made be placed on any decrease in PDS count rate between 20 and 50 keV.

4. X-ray bursts

The observed bursts (and data gaps during which bursts could have been missed), are consistent with a burst recurrence timescale of between 2.40 and 2.57 hr, i.e. with regular burst occurrence as seen in the EXOSAT observation. This timescale is slightly less than the orbital period of the system and so the bursts appear to "march back" relative to the dips during the observation. During the continuous EXOSAT observation the recurrence interval of the bursts was significantly longer, between 5.30 and 5.43 hr (P89). There were also two bursts during the short ASCA observation separated by 3.05 hr. Although it is tempting to assume that this difference in burst repetition

rate is a consequence of a change in the mass accretion rate, the X-ray luminosity of XB 1323−619 did not appear to change systematically during the 3 observations.

Events for each burst were accumulated from the burst maxima until the intensities reached the quiescence level. Table 3 lists the total count and the exposure in each burst spectrum. The mean intensity of the bursts that occur in dips is $\sim 70\%$ of those outside dips and, as seen in Fig. 1, the peak heights of the bursts in dips vary between $\sim 50\%$ and 90\% of the non-dip burst heights. Since there are so few counts for each burst, it is difficult to perform individual spectral fits.

In order to investigate the spectral properties of the bursts, 3 intensity selected non-dip burst spectra (numbers 3, 4, 5, and 10) were first accumulated with count rates of 2–5, 5–8, and >8 s^{-1}. The non-burst, non-dip continuum was again used for background subtraction. The 3 spectra were fitted with an absorbed blackbody model and the results given in Table 4. The N_H values are consistent with those obtained for the non-dip continuum, and there is an indication of temperature change with burst intensity. A F-test shows that the temperature changes are real compared with the mean temperature in the 3 spectra at confidence $>99.9\%$. Using $R_{bb} = d\sqrt{(f_x/(\sigma T^4_{bb}))}$, where f_x is the flux and d the distance of the source, to estimate the blackbody emission radii for each burst spectrum gives similar values of ~ 3 km, using the temperatures and luminosities, L, given in Table 4.

Previously, bursts in dips have only been observed during the *Ginga* observations of XB 1916−053 when 2 out of 29 bursts occurred in dips. The spectral properties of these have been studied by Smale et al. (1992) and by Yoshida (1993) who proposed that the material responsible for the dipping is temporarily ionized by the bursts. In order to investigate whether this scenario is consistent with the burst spectra presented here, a simple spectral comparison between burst no. 1 and the sum of the non-dip bursts was performed using a spectrum extracted from the peak of each burst in each case. The first burst was chosen since it appears to be most strongly affected of the bursts that occurred in dips. No attempt was made to sum data from the different bursts that occurred in dips, due to differing continuum levels.
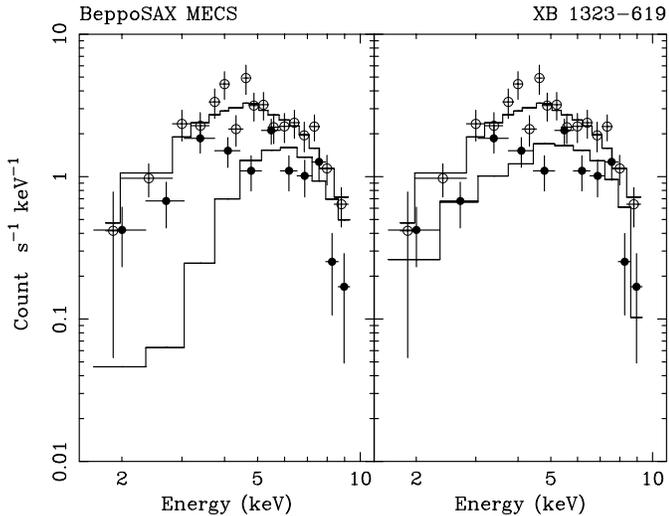
Fig. 6. Fits to MECS summed out of dip bursts (open circles) and to burst no. 1 that occurred during a dip (filled circles). In both panels the out of dip burst spectra are fitted with an absorbed blackbody model. The left panel shows a fit to the burst no. 1 spectrum with the absorption of 3×10^{23} atom cm^{-2} and is clearly inconsistent. The right panel shows a fit to the same spectrum using an ionized absorber

Table 4. Intensity selected non-dip burst spectral fit parameters. 90% confidence limits are given. The luminosity values are bolometric and assume a distance of 10 kpc

Intensity (count s^{-1})	Total count	N_H (10^{22} cm^{-2})	kT_b (keV)	Mean L (erg s^{-1})	χ^2/dof
>8	965	$3.0^{+1.5}_{-1.3}$	2.00 ± 0.22	2.2×10^{37}	37/41
5–8	485	$3.3^{+3.1}_{-2.6}$	1.57 ± 0.22	8.9×10^{36}	18/23
2–5	519	$3.4^{+3.0}_{-2.2}$	1.46 ± 0.24	3.5×10^{36}	38/31

body is covered rapidly and the extended emission is covered progressively as the depth of dipping increases. This becomes the third dipping source with an unabsorbed part of the spectrum that has been modelled in this way (with XB 1916-053 and EXO 0748-676; Church et al. 1998a,b). The systematic increase in covering fraction is consistent with a large absorber moving across the emission regions. The extended nature of the non-thermal Comptonized component is, of course, strongly indicated by the need for progressive covering of this component to explain the spectral evolution during dips, and this is also true in the other sources explained by progressive covering. The identification of the extended emission component with emission from the ADC is supported, for example, by application of this model to EXO 0748−676, in which it was necessary to add a line at 0.65 keV to the extended emission component, the line most probably originating in the ADC (Church et al. 1998a). The column density for the blackbody increases rapidly implying a point source, and to much higher values than for the non-thermal emission consistent with the point source being obscured by higher density regions in the absorber, whereas the extended emission measures an average across the absorber. The break energy of ∼45 keV is somewhat lower than the value found in XB 1916−053. This implies an electron temperature in the Comptonizing region of ∼17 keV.

The fits to the dip spectra clearly show that the covering fraction rises to only ∼ 67% in deepest dipping in the total MECS band, unlike in the sources XB 1916−053 and EXO 0748−676 in which the covering fraction determined in the same way often reaches ∼100% in deepest dipping (Church et al. 1997, 1998a,b).

We have investigated whether this difference may be related to dust scattering given the non-dip column density in XB 1323−619 of ∼ 4×10^{22} atom cm^{-2} compared with 3.2×10^{21} atoms cm^{-2} in XB 1916-053 (Church et al. 1998b) and 1.6×10^{21} atoms cm^{-2} in EXO 0748-676 Church et al. (1998a). This high absorption will result in a substantial dust scattering halo around XB 1323−619 (e.g., Predehl & Schmitt 1995), unless it is intrinsic to the source. For the observed N_H the optical extinction, A_ν, is expected to be ∼14 mag. Using the relation for the dust scattering optical depth, τ_{sca}, derived by Predehl & Schmitt of $\tau_{sca} = 0.087 \times A_\nu \times E_{(keV)}^{-2}$ gives $\tau_{sca} = 0.3$ at 2 keV, or 0.05 at 5 keV. The fractional halo intensity, I_{frac}, is given by $1 - \exp(-\tau_{sca})$ and is 25% at 2 keV, or 5% at 5 keV. The intensity of any scattered halo will not reflect short-term changes in the intensity of the central source since such vari-

and the difficulty in reliably estimating the continuum level to be subtracted, due to the high variability during dipping intervals. The results are shown in Fig. 7. In both panels the summed spectrum is well fitted with an absorbed blackbody. The left panel also shows the best-fit to burst no. 1 using a blackbody with absorption fixed at 3×10^{23} atom cm^{-2}, a value much less than those we obtained in dip fitting (see Table 2). As can be seen, such a column density is strongly inconsistent with the burst spectrum, providing too much absorption. In constrast, the right panel shows a fit using a highly ($\xi \gtrsim 1000$) ionized absorber which matches the data well. This suggests that an ionized absorber is an explanation of the lack of strong absorption for the bursts in dips.

5. Discussion

We have observed XB 1323−619 in a very broad energy range using BeppoSAX. As was found in the BeppoSAX observation of the dipping LMXB XB 1916-053 (Church et al. 1998b), the spectrum of XB 1323−619 extends towards the highest energies of the PDS. BeppoSAX has allowed rigorous testing, for the first time, of absorbed + unabsorbed modelling, and we have shown that the large change in normalization required in the unabsorbed component is inconsistent with the relatively small upper limit decrease of $10 \pm 10\%$ in the PDS intensity above 20 keV, and so this model cannot fit the broadband spectral evolution. However, the non-dip spectrum is well fitted by the two-component model consisting of point-like blackbody emission from the surface or boundary layer at the surface of the neutron star, plus extended Comptonized emission from an Accretion Disk Corona. The dip spectra can be well fitted by the progressive covering model in which the point-source black-

ability is smoothed by differential time delays of up to days (see e.g., Bode et al. 1985). During the ∼1 hr duration dipping intervals the scattering halo will remain visible and its intensity and spectrum will be determined by the mean spectrum of XB 1323−619 over the last days, as well as the properties of the dust grains themselves. However, this assumes that all of the halo is collected requiring extraction of data from a relatively large circular region centred on the source in the imaging instruments compared with the radii actually used (4′ for MECS), so that the amount of halo collected may be substantially less than calculated above. Inspection of Fig. 4 shows that the depth of dipping is ∼65% at 2 keV (for the deep dip spectrum), although the maximum depth of dipping in the light curve will be somewhat greater because of the averaging involved in accumulating the deep dip spectrum. However, if we take 35% as an upper limit to the possible contribution of dust scattering at 2 keV, the contributions at higher energies will be reduced by the expected E^{-2} dependence, and the contribution integrated over the band 2–10 keV can be estimated as < 10%. Thus, it is unlikely that dust scattering can explain the fact that the covering fraction does not exceed 67% in this band. A possible explanation of this is that the absorber is "blobby", such that an appreciable fraction of the absorber consists of lower density regions, which effectively do not cover the emission regions reducing the measured covering fraction f. The measured value of f will be the product of two terms: $f_{\mathrm{env}} \cdot f_{\mathrm{blob}}$, where f_{env} is the covering fraction between the envelope of the source and the extended emission region, and f_{blob} is the partial covering fraction in the overlapping, blobby absorber. Alternatively, the total angular extent of the absorber could be less than that of the extended emission region. However, if the preliminary result that the depth of dipping at the lowest energies reaches 100% is correct, given the poor statistics of this result, then the absorber has to be larger than the source. Further work is needed to clarify this point.

The fits to the cutoff power-law and blackbody model indicate that the blackbody emission has a luminosity of 2.6×10^{35} erg s^{-1}, for an assumed distance of 10 kpc. However, the blackbody is weak and the uncertainties in kT_{bb} may be larger than shown in Table 1. The blackbody comprises 14% of the 2–10 keV flux and the blackbody radius R_{bb} is 0.45 km suggesting that this emission originates in a small boundary layer on the neutron star where the accretion disk impacts. Rutledge et al. (1999) however, have shown that a simple blackbody model may underestimate the emitting area. The total 1–10 keV luminosity is 1.9×10^{36} erg s^{-1}. These values may be compared with recent results from BeppoSAX for XB 1916−053 in which the blackbody luminosity was 5×10^{35} erg s^{-1}, the blackbody 20% of the 1–10 keV flux, the blackbody radius 0.76 km and the total 1–10 keV luminosity 3×10^{36} erg s^{-1} (Church et al. 1998b). It can be seen that the luminosities are scaled down in XB 1323−619 by about a factor of 2 compared with XB 1916−053, with an equivalent change in blackbody radius. The diameter of the extended emission component d_{ADC} can be estimated from the dip ingress and egress timescales ∼250–500 s. Assuming that the absorber is more extended than the source region, d_{ADC} is given by $2\,\pi\,r_{\mathrm{disk}}\,\Delta t/P$ where Δt is the transition time, r_{disk} is the radius of the accretion disk and P is the orbital period. For Δt equal to 250–500 s, d_{ADC} is 4–8×10^9 cm, assuming a disk radius of 3×10^{10} cm.

The bursts occurring in dips provide burst and absorber diagnostics that are not normally available. Previously, 2 bursts in dips have been observed in the *Ginga* observations of XB 1916−053 (Smale et al. 1992; Yoshida 1993). The bursts were not heavily absorbed, which Smale et al. and Yoshida attribute to the almost instantaneous ionization of the material responsible for the dipping. This material then returned to its equilibrium state on the same time scale as the burst decay. Smale et al. (1992) demonstrate that the burst fluence is sufficient to cause significant photoionization at the outer radius of the disk of 1×10^{10} cm in the case of XB 1916−053. In XB 1323−619 the calculated radius of the accretion disk r_{disk} is $\sim 3 \pm 1 \times 10^{10}$ cm. A value of the ionization parameter, $\xi = L/nr^2 \gtrsim 500$ is required for absorption to be markedly reduced compared with a neutral absorber, where r is the distance of the obscuring material from the central X-ray source and n its density. If the absorbing region has a thickness along the line of sight of $\epsilon \cdot r_{\mathrm{disk}}$, then $\xi = L\,\epsilon/N_{\mathrm{H}}\,r_{\mathrm{disk}}$ where N_{H} is the column density due to the absorber, not including interstellar absorption. The value of ϵ is difficult to assess, but values of 0.1 have been suggested (e.g. Mason et al. 1985). However, in the present case, dipping lasts 40% of the orbital cycle implying a very extended absorber, and it is possible that ϵ could be as much as 0.3. The mean burst luminosity close to the peaks of the bursts is 2.7×10^{37} erg s^{-1}. Spectral fitting gives values for N_{H} as an average across the absorbing region of $\sim 20 \times 10^{22}$ atom cm^{-2} after subtraction of the interstellar contribution (see Table 2). Thus the mean value of ξ, equivalent to the mean column density for the absorber, is ∼500 for $\epsilon = 0.1$, and 1500 for $\epsilon = 0.3$. It thus appears likely, given the large uncertainties in this calculation, in L, r_{disk} and ϵ, that the absorber is substantially ionized during bursts so that bursts in dips will not show a strong increase in absorption.

In this case, the reduction of integrated count of ∼30% of the burst in the dip (compared with non-dip bursts) will be due to electron scattering. For the first burst which coincides with a dip, the intensity is 9 count s^{-1} compared with a height of 17 count s^{-1} for the non-dip bursts. This reduction requires an electron column density N_e of $\sim 100 \times 10^{22}$ electron cm^{-2}. This value can be compared with values of the column density for the blackbody in dipping, i.e. the column density applicable to the point-source neutron star, which should provide the electron column density applicable to bursts on the neutron star. However out of bursts, using the maximum N_{H} of the extended emission component as the average of the absorber ($\sim 25 \times 10^{22}$ atom cm^{-2}; Table 2), the average ξ of the absorber is ∼25 showing that hydrogen is ionized. The reduction in intensity that this would cause due to electron scattering is ∼15%, which would be difficult to detect as a vertical shift in PDS data (between non-dip and deep dip) but is consistent with our upper limit of $10 \pm 10\%$ between 20 and 50 keV. The consequence of this is that during a burst, the other

elements may become fully ionized, but the electron density n_e would increase less than 20% assuming Solar abundances. The burst referred to occupied the second half of the dip containing it, so the appropriate column density will be less than the maximum blackbody value, and we estimate 500–1000×10^{22} atom cm^{-2} may be appropriate. Thus the extra N_e may be $\sim 150 \times 10^{22}$ electrons cm^{-2}. This compares well with the value required to reduce the burst intensity as observed.

References

Anders E., Grevesse N., 1989, Geochimica et Cosmochimica Acta 53, 197

Angelini L., Church M.J., Parmar A.N., Bałucińska-Church M., Mineo T., 1998, A&A 339, L41

Bode M.F., Priedhorsky W.C., Norwell G.A., Evans A., 1985, ApJ 299, 845

Boella G., Chiappetti L., Conti G., et al., 1997, A&AS 122, 327

Church M.J., Bałucińska-Church M., 1993, MNRAS 260, 59

Church M.J., Bałucińska-Church M., 1995, A&A 300, 441

Church M.J., Dotani T., Bałucińska-Church M., et al., 1997, ApJ 491, 388

Church M.J., Bałucińska-Church M., Dotani T., Asai K., 1998a, ApJ 504, 516

Church M.J., Parmar A.N., Bałucińska-Church M., et al., 1998b, A&A, 338, 556

Courvoisier T.J.-L., Parmar A.N., Peacock A., Pakull M., 1986, ApJ 309, 265

Forman W., Jones C., Cominsky L., et al., 1978, ApJS 38, 357

Frontera F., Costa E., Dal Fiume D., et al., 1997, A&AS 122, 371

Jonker P.G., van der Klis M., Wijnands R., 1999, ApJ, in press

Manzo G., Guarrusso S., Santangelo A., et al., 1997, A&AS 122, 341

Mason K.O., Parmar A.N., White N.E., 1985, MNRAS 216, 1033

Morrison D., McCammon D., 1983, ApJ 270, 119

Parmar A.N., White N.E., 1988, In: Pallavacini R., White N.E. (eds.) X-ray Astronomy with EXOSAT. Journal of the Italian Astronomical Society 59, p. 147

Parmar A.N., White N.E., Giommi P., Gottwald M., 1986, ApJ 308, 199

Parmar A.N., Gottwald M., van der Klis M., van Paradijs J., 1989, ApJ 338, 1024

Parmar A.N., Martin D.D.E., Bavdaz M., et al., 1997, A&AS 122, 309

Predehl P., Schmitt J.H.M.M., 1995, A&A 293, 889

Rutledge R.E., Bildsten L., Brown E.F., Pavlov G.G., Zavlin V.E., 1999, ApJ, in press

Smale A.P., 1995, AJ 110, 1292

Smale A.P., Mukai K., Williams O.R., Jones M.H. Corbet R.H.D., 1992, ApJ 400, 330

Stark A.A., Gammie C.F., Wilson R.W., et al., 1995, ApJS 79, 77

Tanaka Y., Inoue H., Holt S.S., 1994, PASP 46, L37

Van der Klis M., Jansen F., van Paradijs J., Stollman G., 1985, Space Sci. Rev. 30, 512

Warwick R.S., Marshall N., Fraser G.W., et al., 1981, MNRAS 197, 865

White N.E., Swank J.H., 1982, ApJ 253, L61

Yoshida K., 1993, Thesis, Tokyo University